AGU PUBLICATIONS

JGR

Journal of Geophysical Research: Space Physics

RESEARCH ARTICLE

10.1002/2016JA023825

Carbon dioxide trends in the mesosphere and lower thermosphere

Liying Qian[1], Alan G. Burns[1], Stanley C. Solomon[1], and Wenbin Wang[1]

[1]High Altitude Observatory, National Center for Atmospheric Research, Boulder, Colorado, USA

Key Points:
- Deseasonalizing methods can have significant effects on the derivation of trends
- The registration of profiles in pressure versus altitude coordinates and data quality indicators can also affect the derivation of trends
- The difference between the trend of CO_2 above its homopause and the trend in the lower atmosphere is not statistically significant

Correspondence to:
L. Qian,
lqian@ucar.edu

Citation:
Qian, L., A. G. Burns, S. C. Solomon, and W. Wang (2017), Carbon dioxide trends in the mesosphere and lower thermosphere, *J. Geophys. Res. Space Physics*, *122*, 4474–4488, doi:10.1002/2016JA023825.

Received 19 DEC 2016
Accepted 21 MAR 2017
Accepted article online 25 MAR 2017
Corrected 23 APR 2017
Published online 1 APR 2017

This article was corrected on 23 APR 2017. See the end of the full text for details.

Abstract We investigated trends of carbon dioxide (CO_2) in the upper atmosphere, using data from the Atmosphere Chemistry Experiment Fourier Transform Spectrometer and from the Sounding of the Atmosphere using Broadband Emission Radiometry. Recent analyses of these measurements had indicated that CO_2 above approximately 90 km appeared to be increasing about twice as fast as it was in the lower atmosphere. Models could not reproduce this differential CO_2 trend, calculating instead that the proportional CO_2 increase is approximately constant with altitude. We found three issues with the methodologies used to derive trends from CO_2 profiles: the way that seasonal changes and sampling are accounted for in the analysis, referred to as deseasonalizing; the registration of profiles in pressure versus altitude coordinates; and data quality indicators. Each of these can have significant effects on the derivation of trends. We applied several deseasonalizing procedures, using both pressure and altitude coordinates, also used a time series fit without deseasonalizing, and applied data quality filters. The derived trends were approximately constant with pressure or altitude, about 5.5% per decade, consistent with lower atmosphere CO_2 trends, and consistent with model calculations. We conclude that the difference between the trend of CO_2 above the CO_2 homopause and the trend in the lower, well-mixed atmosphere is not statistically significant.

Plain Language Summary Carbon dioxide (CO_2) has been increasing in the atmosphere where we live, at an average rate of about 5.5% per decade in the past several decades. This increase of CO_2 causes a global warming effect here, but this same increase of CO_2 causes a global cooling effect in the space where low Earth orbit satellites fly. Is the rate of CO_2 increase the same in the space, or is CO_2 increasing twice as fast in the space as it does down here, as suggested by some recent research? This question is important since the rate of CO_2 increase determines the rate of cooling it causes in the space. The more cooling, the less drag that space objects encounter; consequently, more space junks accumulate in the space environment. We investigated the rate of CO_2 increase in the space based on recent satellite observations. We found that the rate of CO_2 increase is approximately constant with altitude, at about 5.5% per decade in the space, the same as the rate of CO_2 increase in the atmosphere where we live.

1. Introduction

Carbon dioxide (CO_2) altitude profiles in the mesosphere and lower thermosphere (MLT) region have been obtained from measurements made by the Atmospheric Chemistry Experiment Fourier Transform Spectrometer (ACE-FTS) on board the Science Satellite 1 (SCISAT-1) during the period from April 2004 to 2016, and by the Sounding of the Atmosphere using Broadband Emission onboard the Thermosphere Ionosphere Mesosphere Energetics Dynamics satellite (TIMED/SABER) from 2002 to 2016. Recent analyses using these two data sets indicate that CO_2 from ~90 to 105 km seems to be increasing faster than the rate of CO_2 increase in the lower, well-mixed atmosphere. At ~100 km, CO_2 trends obtained from ACE-FTS data were ~ 9–12%/decade, which is about twice as large as the anthropogenic rate of increase in CO_2 in the lower atmosphere [*Emmert et al.*, 2012; *Garcia et al.*, 2016]. The average CO_2 trend in the lower atmosphere is ~5%/decade for the most recent decades. CO_2 trends derived from SABER measurements appeared to confirm the results obtained from ACE-FTS [*Yue et al.*, 2015]. Current state-of-the-art upper atmosphere general circulation models and whole atmosphere models, however, cannot reproduce this altitude differential CO_2 trend [*Emmert et al.*, 2012; *Yue et al.*, 2015; *Garcia et al.*, 2016].

This would pose challenges to our current understanding of dynamics, energetics, and photolysis in the mesosphere and lower thermosphere region. The CO_2 volume mixing ratio (vmr) in the MLT region is determined by circulation, eddy mixing, molecular diffusion, and photolysis: these are the processes that are included in current physics-based general circulation models. If these models cannot reproduce the derived faster rate of CO_2 increase in this region, then the models may not be representing these physical processes correctly, or perhaps there are some physical processes that are missing in the models. In addition, since infrared radiation of CO_2 causes the thermosphere to cool and contract, increasing CO_2 drives secular changes in the thermosphere and ionosphere [e.g., *Roble and Dickinson*, 1989; *Akmaev et al*., 2006; *Laštovička et al*., 2006a, 2006b, 2012; *Qian et al*., 2006, 2008, 2011, 2013, 2014; *Solomon et al*., 2010, 2011, 2013, 2015]. A larger rate of increase in CO_2 should cause more rapid changes in the thermosphere and ionosphere. Therefore, quantifying CO_2 trends above the CO_2 homopause is critical for our understanding of dynamics, energetics, and photolysis in the MLT region, and global change in the thermosphere and ionosphere.

One possible cause of a greater CO_2 trend in the MLT region could be a significant trend in eddy mixing. Modeling studies indicated that simulations could resemble the derived altitude differential CO_2 trend if a ~15%–30%/decade increase in eddy mixing was applied [*Emmert et al*., 2012; *Yue et al*., 2015; *Garcia et al*., 2016]. However, a large increase in eddy mixing requires a significant change in atmospheric dynamics, such as gravity wave sources in the troposphere or their propagation through the middle atmosphere, and would have significant implications for the dynamics and composition of the stratosphere, mesosphere, and lower thermosphere. In addition, an increase in eddy mixing should increase the homopause height of CO_2, i.e., the location of the "knee" in the CO_2 vmr profile where it starts to transition from fully mixed to diffusively separating.

We have used a variety of trend analysis methods to look into the trends of CO_2 using both ACE-FTS and SABER measurements. These analysis methods do not exhaust all possible analysis techniques, but they include the techniques that were used in the current literature regarding CO_2 trends in the MLT region, as well as some simple trend analysis methods that require fewer assumptions. The purpose of these analyses is to find out whether the CO_2 trend above the CO_2 homopause is significantly larger than that in the lower, well-mixed atmosphere.

Section 2 briefly describes CO_2 and CO measurements by ACE-FTS and CO_2 measurements by SABER. Section 3 presents various analysis methods and the resulting CO_2 trends. Section 4 examines the vertical profiles of the CO_2 vmr from SABER and ACE-FTS measurements, the CO_2 homopause height and scale height from the CO_2 data, and physical processes that control the CO_2 homopause height and scale height; section 5 summarizes and concludes this study.

2. CO_2 and CO Measured by ACE-FTS and CO_2 Measured by SABER

The SCISAT-1 satellite was launched on 12 August 2003 into a 74° inclination circular orbit at an altitude of 650 km. The primary instrument is the ACE-FTS, which measures limb infrared absorption spectra from solar occultation. A maximum of 15 sunrise profiles and 15 sunset profiles are obtained each day, with coverage weighted toward high latitudes. Although local time and latitude coverage are limited, measurements are not affected by nonlocal thermodynamic equilibrium processes, as is the case for infrared radiation emissions [*Rezac et al*., 2015]. Only fundamental bands were used for the retrievals of CO_2 and CO. ACE-FTS retrievals are registered on a fixed altitude grid but the data set also includes pressures for each profile derived from the retrieved temperatures. The CO_2 vmr is retrieved in the altitude range of 50–120 km, and CO is retrieved from 8 km to ~100 km. ACE-FTS level 2 data version 3.5 from 2004 to 2013 was used in this study. *Bernath et al*. [2005], *Boone et al*. [2013], and *Beagley et al*. [2010] describe in detail ACE-FTS measurements and retrievals of CO_2 and CO vmr.

The TIMED satellite was launched on 7 December 2001 into a 74.1° inclination orbit at 630 km altitude. The SABER infrared sensors perform limb scans that provide simultaneous radiance profiles in 10 spectral channels over the range of 1.27–17 μm, with about 1400 profiles a day [*Russell et al*., 1999]. The latitude coverage is 82°N–54°S or 54°N–82°S, with alternating coverage due to the spacecraft's 60 day sampling cycle. The SABER channels include CO_2 emission bands at 4.3 μm and 15 μm. A two-channel algorithm (4.3 μm and 15 μm narrow band) was used to simultaneously retrieve profiles of kinetic temperature T_k and CO_2 vmr from daytime radiance measurements, in the altitude range of 65–110 km [*Rezac et al*., 2015]. Similar to ACE-FTS, SABER data are also delivered on a fixed altitude grid but include pressures derived from retrieved temperatures. Detailed descriptions of the SABER instrument and data retrieval can be found in *Russell et al*. [1999], *Remsberg et al.* [2008], and *Rezac et al.* [2015]. SABER data version 2.0 from 2002 to 2016 was used in this study.

3. Trends Analysis Methods and Results

3.1. Description of Previous Analysis Techniques

CO_2 trends were analyzed in recent studies by first removing seasonal-latitudinal sampling variations in the data ("deseasonalizing") and then obtaining secular changes using multiple linear regressions (MLRs) to the deseasonalized residuals [*Emmert et al.*, 2012; *Yue et al.*, 2015; *Garcia et al.*, 2016]. Therefore, it is a two-step approach. We note that atmospheric trend analyses often conduct MLR to the actual data time series that include seasonal terms along with the trend term and other relevant terms, which is a one-step process [e.g., *Stiller et al.*, 2012; *Vigouroux et al.*, 2015]. The recent CO_2 trend analyses used the two-step approach, likely due to the unique seasonal-latitudinal sampling patterns in ACE-FTS and SABER observations. The SCISAT-1 and TIMED satellites have very similar orbits (section 2); consequently, both ACE-FTS and SABER have a ~61 day solar time sampling period. Figure 1 shows ACE-FTS seasonal-latitudinal sampling pattern for 2004–2013. *Emmert et al.* [2012] noted that the ACE-FTS seasonal-latitudinal sampling pattern approximately repeats from year to year due to the ~61 day solar time sampling period, which allowed them to isolate the longer-term trends by removing the seasonal-latitudinal dependency of CO_2 and CO from the data. They also provided detailed uncertainty and error analyses of the two-step approach in the supporting information of the paper. The two-step process is described as follows:

1. *Deseasonalizing*. The deseasonalizing methods used in the recent CO_2 trend analyses adopted a similar approach: 1 year (365 days) is divided into a certain number of bins. Examples are 7.6 days ($n = 48$ bins in a year [*Emmert et al.*, 2012]), 30.4 days ($n = 12$ bins in a year [*Garcia et al.*, 2016]), and 60.8 days ($n = 6$ bins in a year). We call this number of days the deseasonalizing window. A grand average of CO_2 vmr for each bin $\left(\overline{\overline{CO_2(i)}}\right)$, $i = 1, 2, \ldots, n$, is calculated using the entire data set. This grand average CO_2 is then subtracted from either the original observed CO_2 time series $CO_2(j)$, $j = 1, 2, \ldots, x$, where x is the number of points in the time series, or an averaged CO_2 time series $CO_2(k)$, $k = 1, 2, \ldots, m$, where m is the number of data points in the averaged time series, and residuals r_{CO_2} are obtained. Examples are monthly averaged CO_2 time series $m = x/30$ and 60 day averaged CO_2 time series $m = x/60$. We call this number of days the averaging window. When the grand average CO_2 is subtracted from an averaged CO_2 time series, then the residuals are as follows:

$$r_{CO_2}(k) = CO_2(k) - \overline{\overline{CO_2(i)}}, \text{ where } k = 1, 2, \ldots, m; \; i = 1, 2, \ldots, n \tag{1}$$

For convenience, we define this method as the "residuals of mean" method since the residuals are obtained from an averaged CO_2 time series. When, instead, the grand average CO_2 is subtracted from the original time series, then the residuals are calculated as follows:

$$r_{CO_2}(j) = CO_2(j) - \overline{\overline{CO_2(i)}}, \text{ where } j = 1, 2, \ldots, x; \; i = 1, 2, \ldots, n \tag{2}$$

The time series $r_{CO_2}(j)$, $j = 1, 2, \ldots, x$ is then averaged to obtain an averaged time series $r_{CO_2}(k)$, $k = 1, 2, \ldots, m$. For convenience, we call this method the "mean of residuals" method since the averaging is done to the residuals. *Emmert et al.* [2012] used the mean of residuals method. They provided a detailed description of the method in the paper, as well as uncertainty and error analyses of the method in the supporting information of the paper. On the other hand, *Yue et al.* [2015] and *Garcia et al.* [2016] used the residuals of mean method.

2. *Multiple linear regressions (MLR)*. A MLR procedure is applied to the residual time series, considering a linear trend in CO_2, dependency on solar cycle variability using the $F_{10.7}$ solar activity index, and in some cases, additional dependency on the quasi-biannual oscillation (QBO) represented by the 30 mb mean zonal wind at the equator [e.g., *Yue et al.*, 2015]. The MLR model used in this study is as follows:

$$r_{CO_2}(t) = a + b \times t + c \times s(t) \tag{3}$$

where t is time. The first term represents a constant residual CO_2, the second term is the linear trend, and the

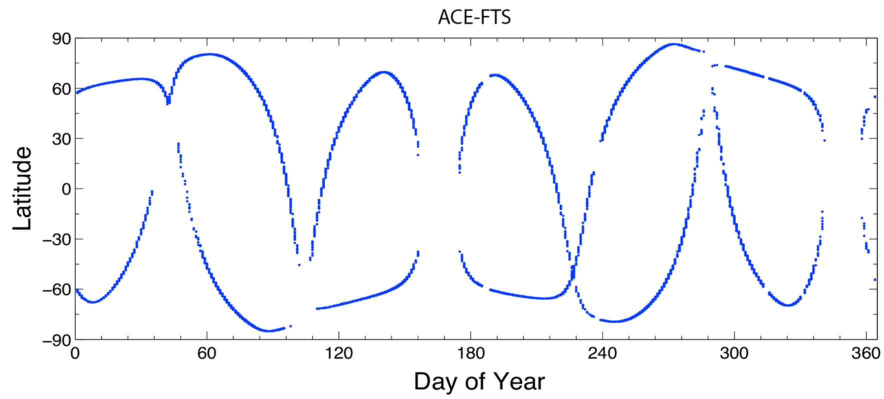

Figure 1. Seasonal-latitudinal sampling pattern of ACE-FTS from 2004 to 2013.

last term is the dependency on solar activity in which *s(t)* is represented by the $F_{10.7}$ index. The QBO was not considered since QBO effects on CO_2 trends in the MLT region are very small [*Yue et al*., 2015; *Garcia et al*., 2016]. Vertical profiles of CO_2 linear trends are then presented in pressure coordinates. Previous studies using these analysis techniques indicated that the CO_2 trend in the attitude range of ~ 90–105 km was about twice as large as the CO_2 trend in the lower, well-mixed atmosphere below about 80 km (~5%/decade), for both ACE-FTS and SABER observations [*Emmert et al*., 2012; *Yue et al*., 2015; *Garcia et al*., 2016]. When we analyzed CO_2 data observed by ACE-FTS and SABER, we found that there are three primary issues that need to be taken into consideration in extracting CO_2 trends from the two data sets.

3.2. Primary Issues in CO_2 Trend Analyses

3.2.1. The Deseasonalizing Process

The first primary issue is the deseasonalizing process, described above. We note here that since ACE-FTS also measures carbon monoxide (CO), trends of CO_x (CO_2 + CO) have been calculated to minimize effects of the solar cycle, and relative trends of CO_x in %/decade have been used to represent relative trends of CO_2 [*Emmert et al*., 2012; *Garcia et al*., 2016]. In this paper, we follow this convention. We calculate relative trends of CO_x and use them to represent relative trends of CO_2 when analyzing the ACE-FTS data set. Since SABER does not measure CO, only CO_2 is used in the analysis.

Figure 2 shows vertical profiles of the ACE-FTS CO_x (CO_2 + CO) relative trends that were calculated using four deseasonalizing methods: (1) Blue: the deseasonalizing window was 30.4 days (12 bins in 365 days); the deseasonalizing procedure was applied to 30.4 day averaged CO_x (residuals of mean). This corresponds to the method used in *Garcia et al*. [2016]. (2) Green: the deseasonalizing window was 60.8 days (6 bins in 365 days); the deseasonalizing procedure was applied to 60.8 day averaged CO_x (residuals of mean). (3) Red: the deseasonalizing window was 30.4 days (12 bins in 365 days); the deseasonalizing procedure was applied to the original CO_x time series; the deseasonalized residuals were then averaged in a 60 day window (mean of residuals). (4) Cyan: the deseasonalizing window was 7.6 days (48 bins in 365 days); the deseasonalizing procedure was applied to the original CO_x time series; the deseasonalized residuals were then averaged in a 60 day window (mean of residuals). This deseasonalizing process was done to each pressure level.

The MLR model in equation (3) was then applied to the residuals obtained from each of the deseasonalizing processes.

Figure 2 demonstrates that the trend results are a function of the deseasonalizing method. Trends produced by the residuals of mean method are sensitive to bin sizes. Method (1) used a deseasonalizing window of 30.4 days, and produced the largest trend, reaching ~ 9%/decade near 100 km. Method (2) used a deseasonalizing window of 60.8 days and produced a different, but still quite large trend. On the other hand, CO_x trends obtained from methods (3) and (4), which used the mean of residuals method, converge, at ~ 6%/decade between ~ 90 km and 105 km, despite the different deseasonalizing bin sizes. The deseasonalizing bin sizes for method (3) and method (4) were 30.4 days and 7.6 days, respectively.

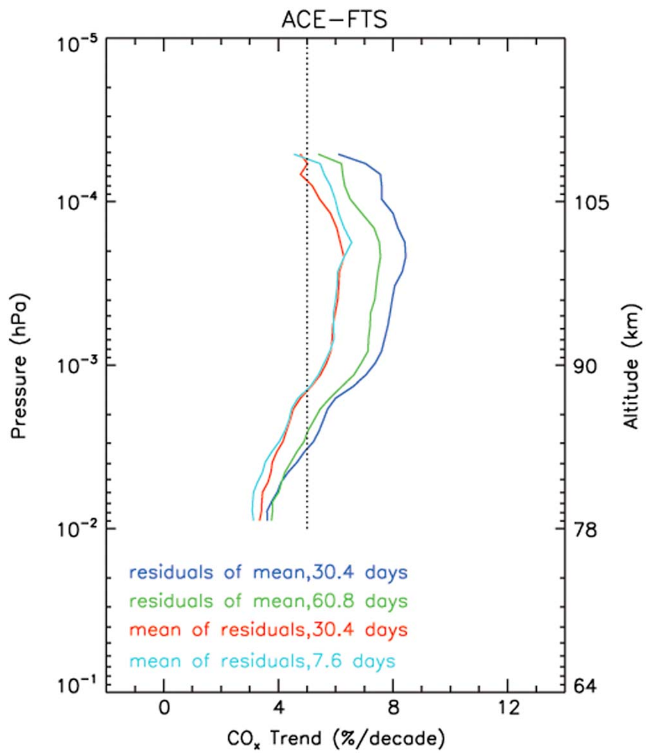

Figure 2. Vertical profiles of CO_x ($CO_2 + CO$) trends obtained using various deseasonalizing techniques, in pressure coordinates, using ACE-FTS data from 2004 to 2013. The right *y* axis shows the approximate altitudes of the pressure surfaces. The black dotted line shows 5%/decade for reference. Blue: the deseasonalizing window was 30.4 days (12 bins in 365 days); the deseasonalizing procedure was applied to 30.4 day averaged CO_x time series. Green: the deseasonalizing window was 60.8 days (6 bins in 365 days); the deseasonalizing procedure was applied to 60.8 day averaged CO_x time series. Red: the deseasonalizing window was 30.4 days; the deseasonalizing procedure was applied to the original CO_x time series; the deseasonalized residuals were then averaged in a 60 day window. Cyan: the deseasonalizing window was 7.6 days (48 bins in 365 days); the deseasonalizing procedure was applied to the original CO_x time series; the deseasonalized residuals were then averaged in a 60 day window.

Figure 3 shows the results for SABER data. Similar to the results for ACE-FTS data shown in Figure 2, there are four vertical profiles of CO_2 trends in Figure 3 using four different deseasonalizing methods: (1) Blue: the deseasonalizing window was 30.4 days (12 bins in 365 days); the deseasonalizing procedure was applied to 30.4 day averaged CO_2. (2) Green: the deseasonalizing window was 60.8 days (6 bins in 365 days); the deseasonalizing procedure was applied to 60.8 day averaged CO_2. (3) Red: the deseasonalizing window was 30.4 days (12 bins in 365 days); the deseasonalizing procedure was applied to the original CO_2 time series; the deseasonalized residuals were then averaged in a 60 day window. (4) Cyan: the deseasonalizing window was 60.8 days (6 bins in 365 days); the deseasonalizing procedure was applied to the original CO_2 time series; the deseasonalized residuals were then averaged in a 60 day window. *Yue et al.* [2015] applied MLR to deseasonalized residuals of 60 day averaged CO_2 observed by SABER; however, they did not state how the 60 day averaged CO_2 was deseasonalized. Again, we see that the trends obtained using the residuals of mean method are sensitive to bin sizes. The trend derived from using the residuals of mean method with a 30.4-day deseasonalizing window produced the largest trend, reaching ~ 10%/decade at 100 km. The trends obtained using the mean of residuals method converge, at ~ 5.5–6% between 90 and 105 km.

The mean of residuals method removes the seasonal, latitudinal, and solar local time sampling variations (the grand averages) from the original time series and then averages the residuals. The residuals of mean method averages the observed time series first, and then it removes the seasonal, latitudinal, and solar time sampling variations from the averaged CO_2 time series. Since the purpose of the deseasonalizing process is to remove the sampling variations of CO_2/CO_x from the observations, it is reasonable to remove the sampling variations from the original observed time series instead of an averaged time series. The mean of residuals method is also the deseasonalizing method used in *Emmert et al*. [2012], which provided a detailed uncertainty and error analyses of the method in the supporting information of the paper. We did many analyses using these two methods, using different bin sizes. As shown in Figures 2 and 3, the results using the residuals of mean method tend to be sensitive to bin sizes, whereas the results using the mean of residuals method converge and are consistent with the result obtained using the nondeseason method that will be introduced later in section 3.3. It is likely that the residual of mean method is sensitive to the bin sizes due to satellite seasonal, latitudinal, and solar time sampling patterns. In this paper, we use the mean of residuals method to deseasonalize the CO_2 data in our analyses.

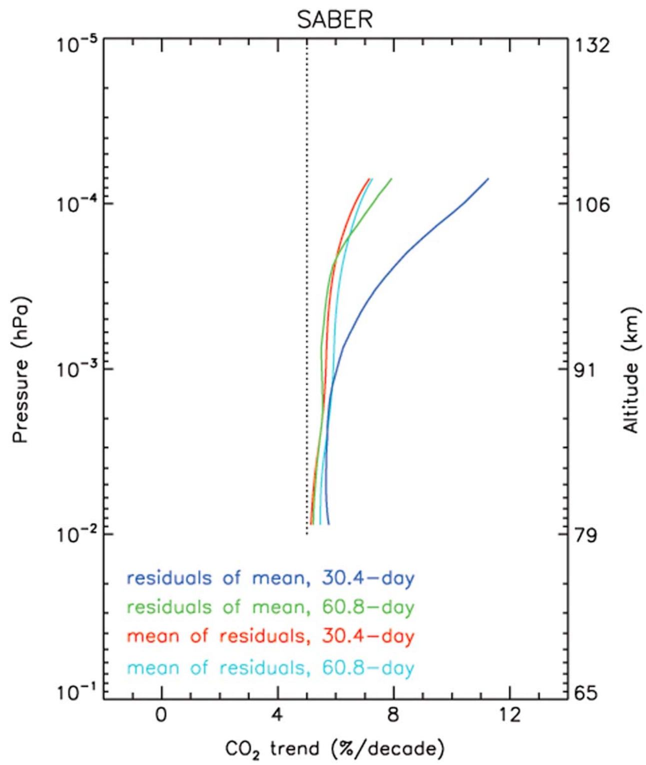

Figure 3. Vertical profiles of CO_2 trends obtained using various deseasonalizing techniques, in pressure coordinates, using SABER data within the latitude range of ±54° from 2002 to 2016. The right *y* axis shows the approximate altitudes of the pressure surfaces. The black dotted line shows 5%/decade for reference. Blue: the deseasonalizing window was 30.4 days (12 bins in 365 days); the deseasonalizing procedure was applied to 30.4 day averaged CO_2 time series. Green: the deseasonalizing window was 60.8 days (6 bins in 365 days); the deseasonalizing procedure was applied to 60.8 day averaged CO_2 time series. Red: the deseasonalizing window was 30.4 days; the deseasonalizing procedure was applied to the original CO_2 time series; the deseasonalized residuals were then averaged in a 60 day window. Cyan: the deseasonalizing window was 60.8 days; the deseasonalizing procedure was applied to the original CO_2 time series; the deseasonalized residuals were then averaged in a 60 day window.

3.2.2. Trends in Altitude Coordinates Versus in Pressure Coordinates

The second primary issue is the difference between a variable expressed in pressure coordinates versus altitude coordinates. A fixed altitude grid and retrieved pressure data are included in both ACE-FTS and SABER data sets. In the recent literature, vertical profiles of CO_2 trends are displayed in pressure coordinates [*Emmert et al.*, 2012; *Yue et al.*, 2015; *Garcia et al.*, 2016]. Here we display CO_2 trends in both altitude and pressure coordinates. Figure 4 shows that in the altitude range of interest (~90–105 km), CO_2 trends in pressure coordinates are larger than those in altitude coordinates. There are two factors that can contribute to this difference.

First, in the Earth's atmosphere, the vertical derivative of a variable "*v*" in altitude coordinates (d*v*/d*z*), as shown in Figure 4a, is usually different from its vertical derivative in log pressure coordinates d*v*/d($-\log_{10}p$), as shown in Figure 4b:

$$\frac{dv}{dz} = \frac{dv}{d(-\log_{10}p)} \times \frac{d(-\log_{10}p)}{dz} \quad (4)$$

Therefore, the value of d($-\log_{10}p$)/d*z* affects how vertical profiles of a variable in altitude coordinates differ from the vertical profiles in pressure coordinates. This value is determined by how atmosphere pressure scale heights change with altitude:

$$\frac{d(-\log_{10}p)}{dz} = -\log_{10}e \times \frac{d\ln p}{dz} = -\log_{10}e \times \frac{d\left(\ln p_0 e^{-\frac{z}{H}}\right)}{dz} = -\log_{10}e \times \left(\frac{z}{H^2}\frac{dH}{dz} - \frac{1}{H}\right) \quad (5)$$

The change of scale height with altitude is determined by the changes of temperature and mean molecular mass with altitude. A decrease in temperature with altitude contributes to a decrease in scale height with altitude, whereas a decrease in mean molecular mass contributes to an increase of scale height with altitude.

Second, in the MLT region, CO_2 cools the atmosphere through infrared cooling at 15 μm; therefore, CO_2 and temperature are coupled [*Chabrillat et al.*, 2002]. The secular increase of CO_2 can drive a temperature trend in the region [e.g., *Beig et al.*, 2003; *Qian et al.*, 2011; *Laštovička et al.*, 2012], which in turn would introduce a trend in the retrieved pressures in the ACE-FTS and SABER data sets. This embedded trend in the pressures can also contribute to the difference in the trends expressed in altitude coordinates versus in pressure coordinates shown in Figure 4.

Since derived trends can depend on the choice of coordinate systems, in this work, we calculate the observed and simulated CO_2 trends in both altitude and pressure coordinates.

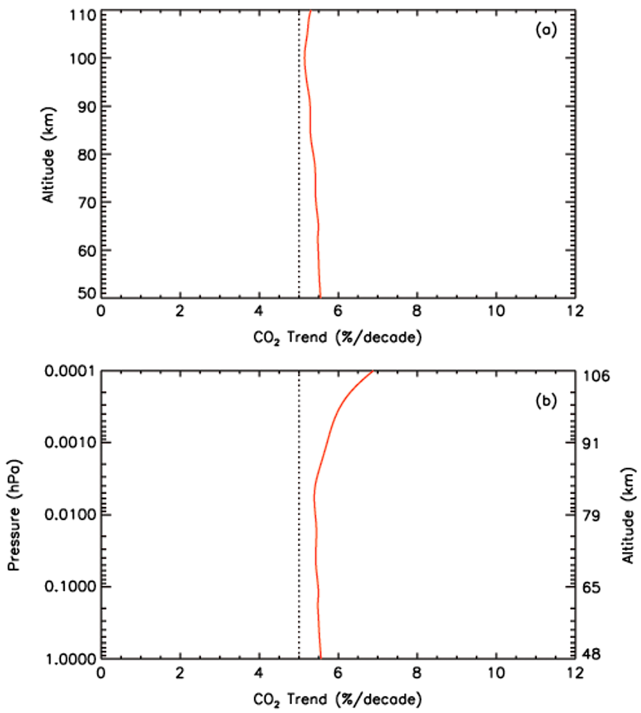

Figure 4. Vertical profiles of CO_2 trends obtained using SABER data within the latitude range of ±54° from 2002 to 2016. The black dotted line shows 5%/decade for reference. (a) CO_2 trends calculated in altitudes coordinates; (b) CO_2 trends calculated in log pressure coordinates, with approximate altitudes of the pressure surfaces shown on the right *y* axis.

3.2.3. Data Quality Flag in ACE-FTS

This issue only applies to ACE-FTS data. There is a data quality flag assigned to each ACE-FTS observation, as shown in Table 1. The data quality flag is an integer ranging from 0 to 9. Quality flag "0" means that the data have no known issues. The other quality flag values indicate that the data have some issue, such as being determined as unnatural outliners, or having instrumental or data processing errors. Figure 5 shows CO_x (CO_2 + CO) absolute trends and relative trends in altitude coordinates (Figures 5a and 5b), and the absolute and relative trends in pressure coordinates (Figures 5c and 5d), calculated using all ACE-FTS data (blue) versus using only data with quality flags equal to 0 (red). All trends were calculated using the mean of residuals method, with a deseasonalizing window of 7.6 days and an averaging window of 90 days for the residuals. This is the method used in *Emmert et al*. [2012]. The relative CO_x trends obtained using all data are about 50% larger than the trends calculated using only data with quality flags equal to 0, either in altitude coordinates or in pressure coordinates. Figure 5 demonstrates that data quality control is very important and makes a significant difference in trend analysis. We note here that in section 3.2.1, we used ACE-FTS data with quality flags equal to 0 for all the results shown in Figure 2.

3.3. Additional Analysis of CO_2 Trends in the MLT Region

Figure 6a shows CO_2 measured by SABER at 96 km, using data in the latitude range of ±54°, and averaged into 60 day bins. The data were binned into 60 day averaged time series since both ACE-FTS and SABER have a sampling period of ~60 days, which approximately repeats from year to year. This mean CO_2 time series exhibits systematic seasonal variations. Although recent studies used deseasonalizing methods to reduce the effects of seasonal-latitudinal variations on CO_2 trends, the mean CO_2 time series shown in Figure 6a indicate that the data series is long enough to permit a direct application of the MLR method of equation

Table 1. Definition of Flag Values Associated With ACE-FTS Level 2 Data, Adapted From the Document Titled: "Data Usage Guide and File Format Description for ACE-FTS Level 2 Data Version 3.5 ASCII Format" at the ACE-FTS Website (https://databace.scisat.ca/level2/ace_v3.5/)

Flag Value	Definition
0	No known issues with data
1	Percent error is not within 0.01–100%, and no other category of flag applies
2	Not enough data points in the region to do statistical analysis, and percent error is within 0.01–100%
3	Not enough data points in the region to do statistical analysis, and percent error is not within 0.01–100%
4	Moderate unnatural outlier detected from running MeAD, percent error within limits
5	Extreme unnatural outlier detected from EDF, percent error within limits
6	Unnatural outlier detected and percent error is outside of limits
7	Instrument or processing error
8	Error fill value of −888 (data are scaled a priori)
9	Data fill value of −999 (no data)

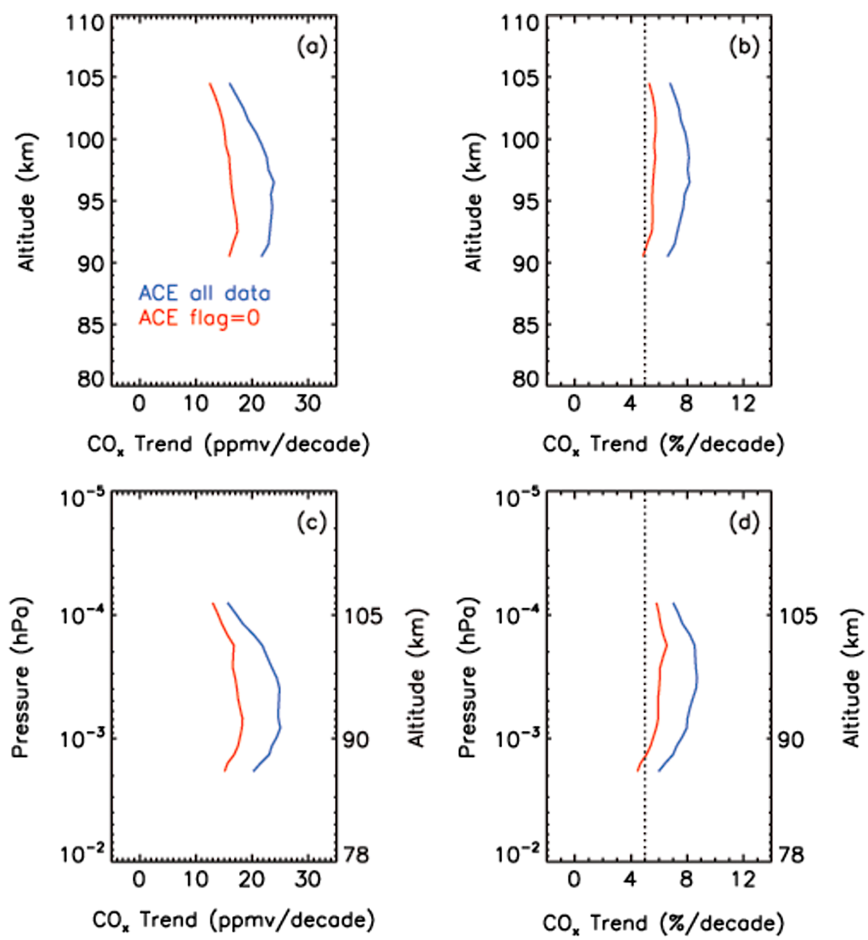

Figure 5. CO_x (CO_2 + CO) trends obtained using ACE-FTS CO_2 and CO data from 2004 to 2013. All trends were calculated using the mean of residuals method, with a deseasonalizing window of 7.6 days and an averaging window of 90 days for the residuals. Blue: CO_x trends calculated using all data. Red: CO_x trends calculated using data with a quality flag that equal to zero. The black dotted line shows 5%/decade for reference. (a) Absolute trends in ppmv/decade in altitude coordinates; (b) relative trends in %/decade in altitude coordinates; (c) absolute trends in ppmv/decade in pressure coordinates; (d) relative trends in %/decade in pressure coordinates.

(3) to the mean CO_2 time series without deseasonalizing. The advantage of this method is that it is simple and straightforward and requires minimal assumptions. We conducted the MLR to the mean CO_2 in Figure 6a. The fitted CO_2 is shown in Figure 6a as the solid line. The CO_2 linear trend at 96 km is 5.2%/decade. In this paper, we will refer to this method as the nondeseason method. This simple analysis shows that CO_2 trend at 96 km is consistent with the trend in the lower atmosphere.

We further compared the CO_2 trends obtained using the nondeseason method to the CO_2 trends obtained using the mean of residuals deseasonalizing method (section 3). Both methods used SABER data that are in the latitude range of ±54°. The deseasonalizing window was 60.8 day. The residuals were then averaged over a 60 day interval. The MLR in equation (3) was applied to the 60 day mean residuals. Figure 6b shows the results from the deseasonalizing method. The SABER CO_2 trends are 5.2%/decade and 5.1%/decade from these two methods, respectively.

Figures 6c and 6d show the corresponding results for ACE-FTS CO_x, using data with quality flags equal to 0, for the period 2004–2013. The ACE-FTS CO_x trends are 6.1%/decade and 5.1%/decade for the nondeseason method and the mean of residuals deseasonalizing method (a 60.8 day deseasonalizing window, and a 60 day averaging window), respectively. Figure 6 demonstrates that the CO_2 and CO_x trends, obtained using the deseasonalizing method, converge with the results using the nondeseason method when the deseasonalizing is done using the mean of residuals method instead of the residuals of mean method (section 3).

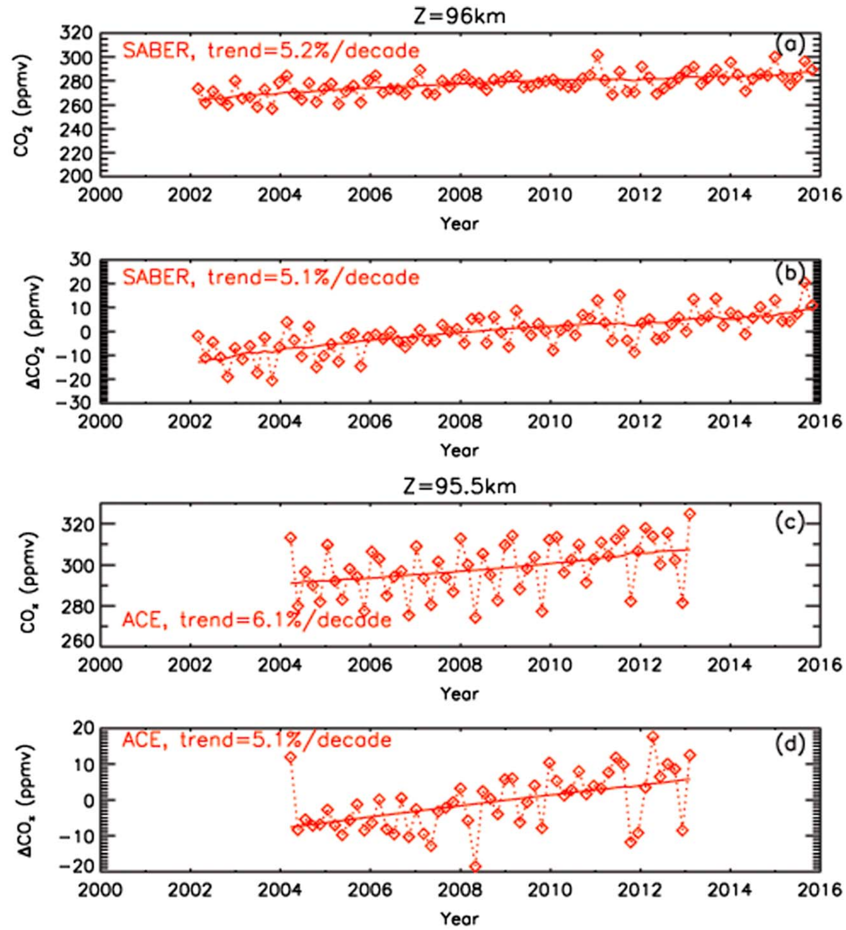

Figure 6. (a) The 60 day averaged CO_2 measured by SABER (red diamond symbols), the MLR fitting of the mean CO_2 (solid line), and CO_2 trend, for the period of 2002–2015, at 96 km; (b) deseasonalized (60.8 day) mean residuals calculated from SABER data (red diamond symbols), the MLR fitting (solid line), and the trend, for the period of 2002–2015, at 96 km; (c) 60 day averaged CO_x measured by ACE-FTS (red diamond symbols), the MLR fitting of the mean CO_x (solid line), and CO_x trend, for the period of 2004–2013, at 95.5 km; (d) deseasonalized (60.8 day) mean residuals (60 day average) calculated from ACE-FTS data (red diamond symbols), the MLR fitting (solid line), and the trend, for the period of 2004–2013, at 95. 5 km.

We note that since ACE-FTS data cover a shorter time period than SABER data, and the ACE-FTS sampling rate is much lower than SABER (~30 profiles per day versus ~ 1400 profiles per day), trend estimation uncertainties (Figures 7a and 7b) using ACE-FTS data, for both the nondeseason and the deseasonalizing methods, are much larger compared to those using SABER data.

Figure 7 shows the vertical profiles of the relative CO_2 trends in %/decade and the trend estimation uncertainties in altitude coordinates, derived from SABER (red) and ACE-FTS (blue) data. We also show CO_x ($CO_2 + CO$) trends derived from the Whole Atmosphere Community Climate Model (WACCM) simulations, which is adapted from *Garcia et al.* [2016], for reference (black). The error bars in Figure 7 show the trend estimation uncertainty at each vertical level, which is calculated as the two standard deviations of the MLR fit (equation (3)) modified by the first-order autocorrelation of the residuals of the fit [*Tiao et al.*, 1990]. SABER results were obtained using data within the latitude range of ±54° from 2002 to 2016. The ACE-FTS results used data with quality flags equal to 0, for the period 2004–2013, and ACE-FTS CO_2 trends are represented by CO_x ($CO_2 + CO$) trends. We used both the nondeseason method (Figure 7a) and the mean of the residuals deseasonalizing method (Figure 7b). The deseasonalizing method is the same as the one used for Figures 6b and 6d. The trend estimation uncertainties using the nondeseason method are larger than those using the deseasonalizing method, presumably due to the seasonal variations in CO_2. However, both methods show that the CO_2 trends in the altitude range of ~ 90 km–105 km are consistent with the CO_2

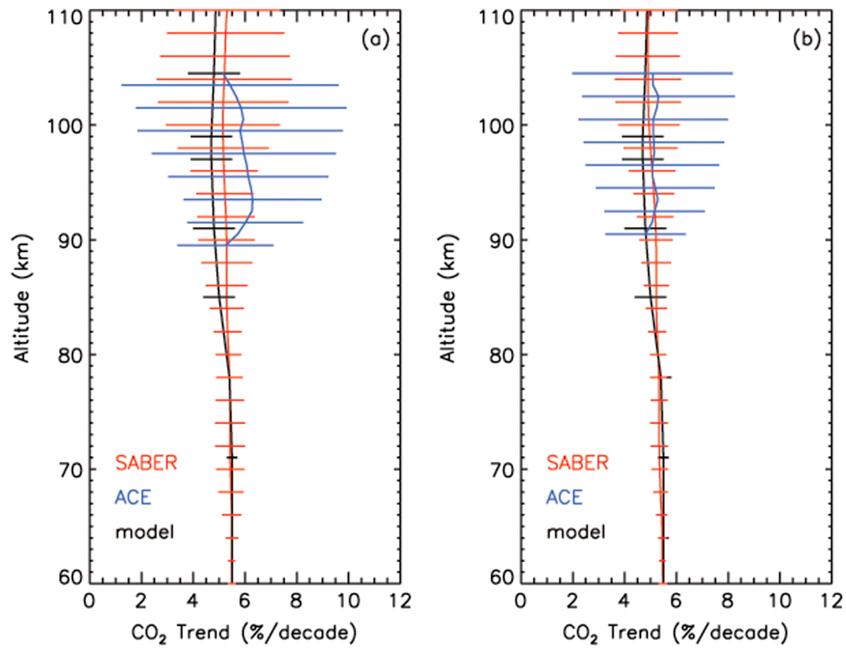

Figure 7. Vertical profiles of the relative CO_2 trends in %/decade in altitude coordinates, obtained from SABER (red) and ACE-FTS (blue) data. SABER results were obtained using data within the latitude range of ±54° from 2002 to 2016. ACE-FTS used data with quality flags that equal to 0, for the period of 2004–2013, and ACE-FTS CO_2 trends are represented by CO_x (CO_2 + CO) trends. The black profiles show CO_x (CO_2 + CO) trends derived from WACCM model simulations, which is adapted from *Garcia et al*. [2016] for reference. The horizontal bars indicate the trend estimation uncertainty at each vertical level, which is calculated as the two standard deviations of the MLR fit modified by the autocorrelation of the residuals of the fit at each level. (a) Trends obtained using the nondeseason method; (b) trends obtained using the mean of residuals method with a deseasonalizing window of 60.8 days and an averaging window of 60 days for the deseasonalized residuals.

trend in the lower atmosphere, at a rate of ~ 5.5%/decade, based on both SABER and ACE-FTS data. These results are consistent with WACCM results of *Garcia et al*. [2016] (black).

Figure 8 is the same as Figure 7 except that the trends were calculated in pressure coordinates. The trends in pressure coordinates (Figure 8) are larger than the trends in altitude coordinates (Figure 7) from ~ 90 to 105 km. This is true for the trends obtained from both ACE-FTS and SABER data. This difference in the calculated trends in the two coordinate systems is due to the mapping from altitude to pressure, as discussed in section 3.2.2 (Figure 4). Despite this difference, ACE-FTS and SABER data are in agreement that the CO_2 trend in the altitude range of ~ 90–105 km is consistent with the trend in the lower, well-mixed atmosphere and that the difference between the trends in these two altitude regions is statistically insignificant. In addition, the trends derived from ACE-FTS and SABER data are consistent with WACCM results of *Garcia et al*. [2016], shown as reference (black profiles), as well as the modeling results in *Emmert et al*. [2012] and *Yue et al*. [2015].

4. Discussion

CO_2 is well mixed below its homopause, which is around 80–90 km [e.g., *Lopez-Puertas et al*., 2000; *Garcia et al*., 2014; *Rezac et al*., 2015]. Above its homopause, CO_2 vmr decreases exponentially as a result of increased molecular diffusion, decreased eddy mixing, and photolysis of CO_2. In order for the trend of CO_2 above its homopause to be larger than its trend in the lower, well-mixed region, there needs to be a trend in homopause heights with the homopause heights increasing with time, and/or a trend in the slope of CO_2 profiles above its homopause. We examined the observed annual-average CO_2 profiles as a sanity check to see whether they suggest that CO_2 trends in the altitude range of ~ 90–105 km are twice as large as the trends in the lower, mixed atmosphere, or are consistent with the trend results shown in Figures 7 and 8.

Figure 9 shows the annual-average CO_2 vertical profiles observed by SABER, using data within the latitude range of ±54°, from 2002 to 2015. We present the vertical profiles in both altitude and pressure

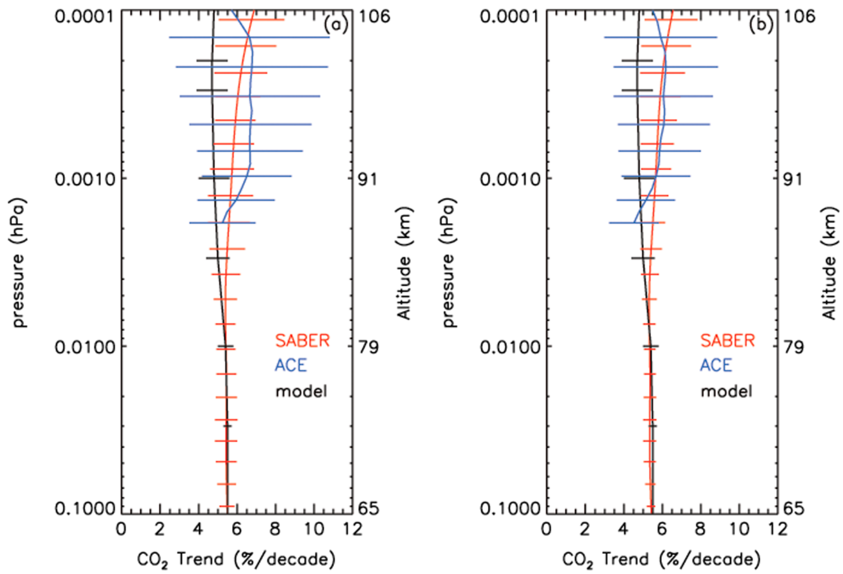

Figure 8. Vertical profiles of the relative CO_2 trends in %/decade in pressure coordinates, calculated from SABER (red) and ACE-FTS (blue) data. SABER results were obtained using data within the latitude range of ±54° from 2002 to 2016. ACE-FTS used data with quality flags that equal to 0, for the period of 2004–2013, and ACE-FTS CO_2 trends are represented by CO_x ($CO_2 + CO$) trends. The black profiles show CO_x ($CO_2 + CO$) trends derived from WACCM model simulations, which is adapted from *Garcia et al*. [2016] for reference. The horizontal bars indicate the trend estimation uncertainty at each vertical level, which is calculated as the two standard deviations of the MLR fit modified by the autocorrelation of the residuals of the fit at each level. (a) Trends obtained using the nondeseason method; (b) trends obtained using the mean of residuals method with a deseasonalizing window of 60.8 days and an averaging window of 60 days for the deseasonalized residuals.

coordinates. In the case of pressure coordinates, the approximate altitude of each pressure surface is given as the right *y* axis. In both altitude and pressure coordinates, there is no apparent positive trend in the homopause heights. We calculated vertical gradients of the annual-average CO_2 vmr shown in Figure 9 to examine the inflection points where the homopause occurs and found no evidence of a trend in the homopause heights in this 14 year period. We also calculated the scale heights of the yearly averaged CO_2 profiles (Figure 9a) in the 95–100 km altitude region. The scale heights fluctuated between 4.01 km and 4.06 km for these 14 years without a trend. Note that CO_2 may not be in diffusive equilibrium in this altitude region due to photolysis, eddy diffusion, and neutral wind advection. Therefore, the scale heights that we calculated are pseudo scale heights that are used as an indicator of the slopes of the CO_2 profiles.

Figure 10 shows the yearly averaged CO_x ($CO_2 + CO$) profiles from ACE-FTS measurements, for 2004–2012, in both altitude and pressure coordinates. Both sunset and sunrise measurements were used to obtain these yearly averaged CO_x profiles. Similar to the SABER profiles shown in Figure 9, there is no indication of an increase in the CO_x homopause heights over the observing period from 2004 to 2012, in both altitude and pressure coordinates. We calculated pseudo scale heights of the CO_x profiles above the homopause. Again, the scale heights fluctuated in this time period without an apparent trend. For example, at 95–100 km, the pseudo scale heights fluctuated between 4.42 km and 4.47 km from 2004 to 2012.

As mentioned earlier, CO_2 concentrations in the MLT region are determined by vertical and horizontal advection, eddy mixing, molecular diffusion, and photolysis. On a global average basis, the physical process that could change homopause heights would likely be eddy mixing. Note that the mean molecular scale height in the altitude region of 80–90 km is small, ~5 km. Since total number density decreases with altitude very quickly in this region, a significant increase in eddy mixing would be needed to produce an appreciable increase in homopause heights. Numerical tests showed that a ~15%–30%/decade increase in eddy diffusion coefficient would be needed in order to produce a CO_x trend in the 90–105 km altitude region twice of the trend in the lower atmosphere [*Emmert et al*., 2012; *Garcia et al*., 2016].

Above the CO_2 homopause, changes in the temperature and photolysis rate need to be considered. Interannual changes in temperature are possible. Photolysis of CO_2 by ultraviolet radiation becomes

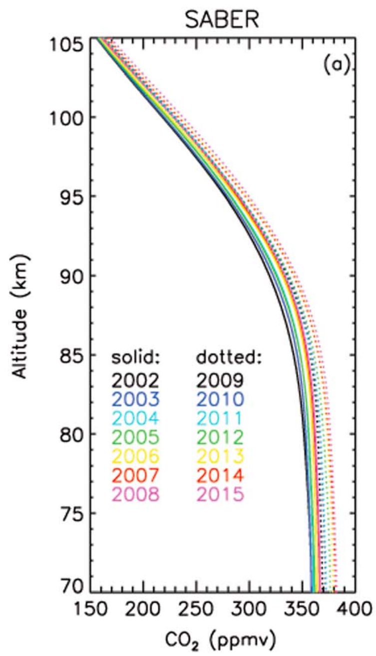

Figure 9. Annual-average CO_2 profiles from SABER measurements for 2002–2015. The CO_2 profiles used SABER data within the latitude range of ±54°. (a) In altitude coordinates; (b) in pressure coordinates, with the approximate altitude for each pressure surface shown on the right *y* axis.

important, and photolysis can cause solar cycle variations in CO_2 concentrations. The solar activity dependence term in equation (3) is in the order of ~ −0.05% per unit $F_{10.7}$ change in the altitude region of ~ 90–105 km. The typical solar cycle variability of the $F_{10.7}$ index is ~ 130 units. Therefore, solar cycle variability of CO_2 is in the order of ~ 7% in the region, with less CO_2 at high solar activity. However, our

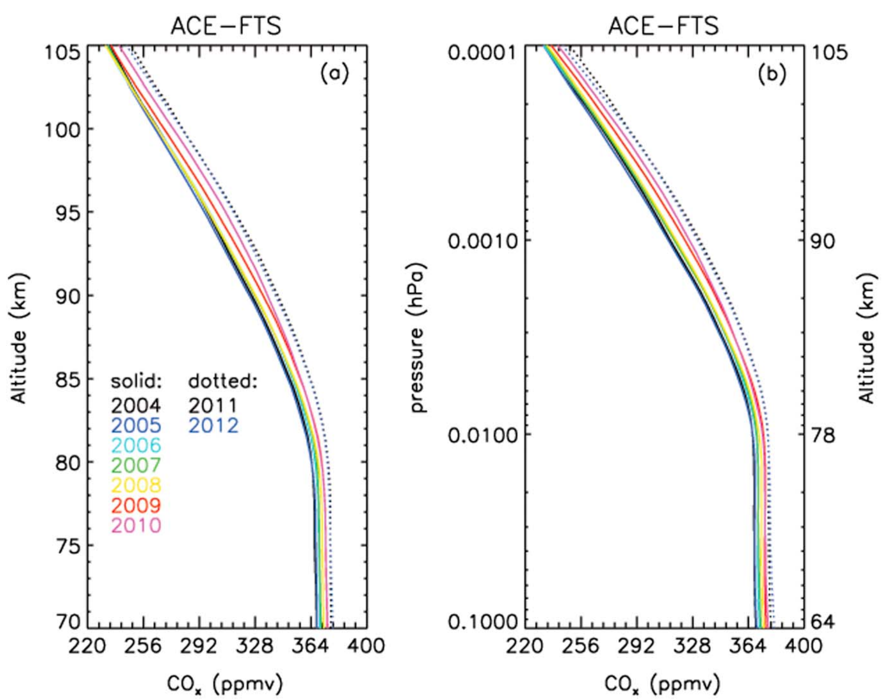

Figure 10. Annual-average CO_x ($CO_2 + CO$) profiles from ACE-FTS measurements for 2004–2012. The CO_x profiles used both sunset and sunrise data with a data quality flag that equal to 0. (a) In altitude coordinates; (b) in pressure coordinates, with the approximate altitude for each pressure surface shown on the right *y* axis.

examination of CO_2 (SABER) and CO_x (ACE-FTS) pseudo scale heights, which include the combined effects from all physical processes including both temperature and photolysis, does not show a trend in the pseudo scale heights at ~90–105 km during the observing periods.

Model simulations by *Garcia et al*. [2016] found that the global trend of CO_x in the lower thermosphere calculated by the WACCM was not significantly different from the trend ascribable to anthropogenic increases in CO_2 in the lower atmosphere, on a percentage basis, and that this trend was nowhere larger than 5.5% per decade. *Emmert et al*. [2012] found a similar result using the National Center for Atmospheric Research (NCAR) Global Mean model of the thermosphere and mesosphere. The analyses presented here are in agreement with these model results, within the uncertainties associated with the retrieval procedures and trend inferences.

5. Summary and Conclusions

Recent studies on CO_2 trends in the MLT region indicated that CO_2 in the altitude region ~ 90–105 km is increasing at a rate of ~ 9–12%/decade, which would be about twice as fast as the rate of the CO_2 increase in the lower, well-mixed atmosphere. These studies are based on observations made by ACE-FTS (2004–2013) and SABER (2002–2016). Model simulations using state-of-art general circulation models could not reproduce this derived altitude differential CO_2 trend. Modeling tests indicated that a substantially large increase in eddy mixing, ~15%–30%/decade, would be needed to bring the simulated CO_2 trend close to the trends derived from the measurements.

CO_2 is well mixed below its homopause, which is ~ 80–90 km. Above its homopause, CO_2 vmr decreases exponentially due to increased molecular diffusion, decreased eddy diffusion, and photolysis. If the trend of CO_2 above the homopause were larger than the trend in the lower atmosphere, then there should be a trend in homopause heights, with the homopause height increasing with time, and/or a trend in the scale height of the CO_2 profile above the CO_2 homopause. CO_2 vertical profiles observed by SABER and CO_x (CO_2 + CO) profiles observed by ACE-FTS, however, show no apparent trend in either the CO_2 homopause height or the scale height.

We investigated the methods used to perform CO_2 trend analysis using ACE-FTS and SABER data and found that there are three primary issues regarding CO_2 trend analysis using these data sets:

1. Recent results of CO_2 trends were obtained using a deseasonalizing process. Our analysis shows that when the deseasonalizing algorithm is applied to an averaged CO_2 time series (residuals of mean), the resulting CO_2 trends are sensitive to deseasonalizing bin sizes, and this method tends to produce a larger CO_2 trend. On the other hand, when the deseasonalizing algorithm is applied to the original observed time series (mean of residuals), the resulting CO_2 trends converge when using different deseasonalizing bin sizes. We consider that it is reasonable to remove the seasonal variations from the original observed time series (mean of residuals) instead of from the averaged CO_2 time series.
2. We found that CO_2 trends calculated in pressure coordinates are larger than when calculated in altitude coordinates. This difference is determined by atmosphere properties including how temperature and mean molecular mass change with altitude, and conceivably with time.
3. ACE-FTS data include a data quality flag, with value zero indicating that the data have no known issues. The CO_2 trend in the ~ 90–105 km region calculated using all data is ~ 50% larger than when calculated using only data with quality flags equal to 0.

ACE-FTS and SABER CO_2 data series are long enough to permit the direct application of the MLR to the observed CO_2 time series instead of to the deseasonalized CO_2 residual time series. We calculated CO_2 trends by applying the MLR to the 60 day averaged CO_2 time series (the nondeseason method). We only used data with a quality flag of zero for ACE-FTS and used data within the latitude range of ±54° for SABER. We also calculated CO_2 trends using the mean of residuals deseasonalizing technique, with a deseasonalizing window of 60.8 days and an averaging window of 60 days for the residuals. These two methods produced convergent and consistent results. In both altitude and pressure coordinates, CO_2 trends obtained using ACE-FTS and SABER data are in good agreement, and the difference between the trends in the altitude range of ~ 90–105 km and in the lower atmosphere is statistically not significant.

On a global average basis, a possible physical process that could change homopause heights would be eddy mixing. Numerical tests by *Emmert et al*. [2012] and by *Garcia et al*. [2016] showed that an ~ 15%–30%/decade increase in the eddy diffusion coefficient would be needed to produce a CO_2 trend in the ~ 90–105 km region of about twice the trend in the lower atmosphere. There is no evidence that this large change in eddy mixing has occurred in the past decade, and no apparent trend was seen in the homopause height or scale height of CO_2 in the SABER and ACE-FTS measurements. This is consistent with model results that show that there should be no differential trend of CO_2 with altitude.

Based on these results, we conclude that the difference between the CO_2 trend in the altitude region ~ 90–105 km and the trend in the lower, well-mixed atmosphere, is not statistically significant. These results are based on ~ 14 years of SABER data and ~ 9 years of ACE-FTS data. Longer data sets would allow us to obtain more robust and definitive trend results.

Acknowledgments
This research was supported by NASA grant NNX16AH06G. We greatly appreciate the SABER team who provided the SABER version 2.0 data. The SABER CO_2 data are available at ftp://saber.gats-inc.com/Version2_0/Level2C/. We thank the ACE-FTS team for providing the ACE-FTS level 2 version 3.5 CO_2 and CO data. The Atmospheric Chemistry Experiment (ACE), also known as SCISAT, is a Canadian-led mission mainly supported by the Canadian Space Agency and the Natural Sciences and Engineering Research Council of Canada. The ACE-FTS level 2 data version 3.5 are available at https://database.scisat.ca/level2/ace_v3.5/. All data that produced the results in this paper are available on NCAR's High Performance Storage System upon request.

References

Akmaev, R. A., V. I. Fomichev, and X. Zhu (2006), Impact of middle-atmospheric composition changes on greenhouse cooling in the upper atmosphere, *J. Atmos. Sol. Terr. Phys.*, *68*, 1879–1889, doi:10.1016/j.jastp.2006.03.008.

Beagley, S. R., C. D. Boone, V. I. Fomichev, J. J. Jin, K. Semeniuk, J. C. McConnell, and P. F. Bernath (2010), First multi-year occultation observations of CO_2 in the MLT by ACE satellite: Observations and analysis using the extended CMAM, *Atmos. Chem. Phys.*, *10*, 1133–1153, doi:10.5194/acp-10-1133-2010.

Beig, G., et al. (2003), Review of mesospheric temperature trends, *Rev. Geophys.*, *41*(4), 1015, doi:10.1029/2002RG000121.

Bernath, P. F., et al. (2005), Atmospheric Chemistry Experiment (ACE): Mission overview, *Geophys. Res. Lett.*, *32*, L15S01, doi:10.1029/2005GLO22386.

Boone, C., K. Walker, and K. Walker (2013), Version 3 retrievals for the atmospheric chemistry experiment Fourier transform spectrometer (ACE-FTS), in *The Atmospheric Chemistry Experiment ACE at 10: A Solar Occultation Anthology*, edited by P. Bernath, pp. 103–127 , A. Deepak Publ., Hampton, Va.

Chabrillat, S., G. Kockarts, D. Fonteyn, and G. Brasseur (2002), Impact of molecular diffusion on the CO_2 distribution and the temperature in the mesosphere, *Geophys. Res. Lett.*, *29*(15), 1729, doi:10.1029/2002GL015309.

Emmert, J. T., M. H. Stevens, P. F. Bernath, D. P. Drob, and C. D. Boone (2012), Observations of increasing carbon dioxide concentration in Earth's thermosphere, *Nat. Geosci.*, *5*, 868–871, doi:10.1038/ngeo1626.

Garcia, R. R., M. López-Puertas, B. Funke, D. R. Marsh, D. E. Kinnison, A. K. Smith, and F. González-Galindo (2014), On the distribution of CO_2 and CO in the mesosphere and lower thermosphere, *J. Geophys. Res. Atmos.*, *119*, 5700–5718, doi:10.1002/2013JD021208.

Garcia, R. R., M. López-Puertas, B. Funke, D. Kinnison, D. Marsh, and L. Qian (2016), On the secular trend of CO_x and CO_2 in the lower thermosphere, *J. Geophys. Res. Space Physics*, *121*, 3634–3644, doi:10.1002/2015JD024553.

Laštovička, J., R. A. Akmaev, G. Beig, J. Bremer, and J. T. Emmert (2006a), Global change in the upper atmosphere, *Science*, *314*, 1253–1254, doi:10.1126/science.1135134.

Laštovička, J., et al. (2006b), Long-term trends in f_oF_2: A comparison of various methods, *J. Atmos. Terr. Phys.*, *68*, 1854–1870, doi:10.1016/j.jastp.2006.02.009.

Laštovička, J., S. C. Solomon, and L. Qian (2012), Trends in the neutral and ionized upper atmosphere, *Space Sci. Rev.*, *168*, 113–145, doi:10.1007/s11214-011-9810-z.

Lopez-Puertas, M., M. A. Lopez-Valverde, R. R. Garcia, and R. G. Roble (2000), A review of CO_2 and CO abundance in the middle atmosphere, *Geophys. Monogr.*, *123*, 83–100.

Qian, L., R. G. Roble, S. C. Solomon, and T. J. Kane (2006), Calculated and observed climate change in the thermosphere, and a prediction for solar cycle 24, *Geophys. Res. Lett.*, *33*, L23705, doi:10.1029/2006GL027185.

Qian, L., S. C. Solomon, R. G. Roble, and T. J. Kane (2008), Model simulations of global change in the ionosphere, *Geophys. Res. Lett.*, *35*, L07811, doi:10.1029/2007GL033156.

Qian, L., J. Laštovička, R. G. Roble, and S. C. Solomon (2011), Progress in observations and simulations of global change in the upper atmosphere, *J. Geophys. Res.*, *116*, A00H03, doi:10.1029/2010JA016317.

Qian, L., D. Marsh, A. Merkel, S. C. Solomon, and R. G. Roble (2013), Effect of trends of middle atmosphere gases on the mesosphere and thermosphere, *J. Geophys. Res. Space Physics*, *118*, 3846–3855, doi:10.1002/jgra.50354.

Qian, L., S. C. Solomon, and R. G. Roble (2014), Secular changes in the thermosphere and ionosphere between two quiet Sun periods, *J. Geophys. Res. Space Physics*, *119*, 2255–2262, doi:10.1002/2013JA019438.

Remsberg, E. E., et al. (2008), Assessment of the quality of the version 1.07 temperature-versus pressure profiles of the middle atmosphere from TIMED/SABER, *J. Geophys. Res.*, *113*, D17101, doi:10.1029/2008JD010013.

Rezac, L., A. Kutepov, J. M. Russell III, A. G. Feofilov, J. Yue, and R. A. Goldberg (2015), Simultaneous retrieval of $T(p)$ and CO_2 VMR for non-LTE limb radiance measured by the SABER/TIMED instrument, *J. Atmos. Sol. Terr. Phys.*, *130–131*, 23–42, doi:10.1016/j.jastp.2015.05.004.

Roble, R. G., and R. E. Dickinson (1989), How will changes in carbon dioxide and methane modify the mean structure of the mesosphere and thermosphere?, *Geophys. Res. Lett.*, *16*, 1144–1441, doi:10.1029/GL016i012p01441.

Russell, J. M., III, M. G. Mlynczak, L. L. Gordley, J. J. Tansock Jr., and R. W. Esplin (1999), Overview of the SABER experiment and preliminary calibration results, *SPIE Proc.*, *3756*, 277–288, doi:10.1117/12.366382.

Solomon, S. C., T. N. Woods, L. V. Didkovsky, J. T. Emmert, and L. Qian (2010), Anomalously low solar extreme-ultraviolet irradiance and thermospheric density during solar minimum, *Geophys. Res. Lett.*, *37*, L16103, doi:10.1029/2010GL044468.

Solomon, S. C., L. Qian, L. V. Didkovsky, R. A. Viereck, and T. N. Woods (2011), Causes of low thermospheric density during the 2007–2009 solar minimum, *J. Geophys. Res.*, *116*, A00H07, doi:10.1029/2011JA016508.

Solomon, S. C., L. Qian, and A. G. Burns (2013), The anomalous ionosphere between solar cycles 23 and 24, *J. Geophys. Res. Space Physics*, *118*, 6524–6535, doi:10.1002/jgra.50561.

Solomon, S. C., L. Qian, and R. G. Roble (2015), New 3-D simulations of climate change in the thermosphere, *J. Geophys. Res. Space Physics*, *120*, 2183–2193, doi:10.1002/2014JA020886.

Stiller, G. P., et al. (2012), Observed temporal evolution of global mean age of stratospheric air for the 2002 to 2010 period, *Atmos. Chem. Phys.*, *12*, 3311–3331, doi:10.5194/acp-12-3311-2012.
Tiao, G. C., G. C. Reinsel, D. Xu, J. H. Pedrick, X. Zhu, A. J. Miller, J. J. DeLuisi, C. L. Mateer, and D. J. Wuebbles (1990), Effects of autocorrelation and temporal sampling schemes on estimates of trend and spatial correlation, *J. Geophys. Res.*, *95*, 20,507–20,517, doi:10.1029/JD095iD12p20507.
Vigouroux, C., et al. (2015), Trends of ozone total columns and vertical distribution from FTIR observations at eight NDACC stations around the globe, *Atmos. Chem. Phys.*, *15*, 2915–2933, doi:10.5194/acp-15-2915-2015.
Yue, J., J. Russell III, Y. Jian, L. Rezac, R. Garcia, M. López-Puertas, and M. G. Mlynczak (2015), Increasing carbon dioxide concentration in the upper atmosphere observed by SABER, *Geophys. Res. Lett.*, *42*, 7194–7199, doi:10.1002/2015GL064696.

Erratum

In the originally published version of this article, equation (5) contained an error: the terms appearing as $\log_{10}^{e}$ should have been represented as $\log_{10}e$. The error has since been corrected, and this version may be considered the authoritative version of record.